

# Spatial distribution of the absorption factor for an infinite cylindrical sample used with a two-dimensional area detector

Sergei Sulyanov,<sup>a,b\*</sup> Andrei Gogin<sup>a,c</sup> and Hans Boysen<sup>d</sup><sup>a</sup>Institute of Crystallography RAS, Leninsky Prospect 59, Moscow 119333, Russian Federation,<sup>b</sup>Kurchatov Centre, Moscow, Russian Federation, <sup>c</sup>Physical Faculty, Moscow State University,Moscow, Russian Federation, and <sup>d</sup>Sektion Kristallographie, Department für Geo- und Umweltwissenschaften, Ludwig-Maximilians-Universität, Theresienstrasse 41, 80333 München, Germany.

Correspondence e-mail: sul942@yandex.ru

Specialized software has been developed to calculate the absorption factor for the infinite-cylinder transmission Debye–Scherrer geometry (including inclined beams) to be used with two-dimensional area powder pattern registration. The diffracted beams are defined by the direction cosines in the laboratory Cartesian coordinate system. Modern two-dimensional area detectors have a large number of pixels, so an interpolation is made by the triangulation procedure to save computer time. The absorption correction is allowed for so that the intensity in each pixel is reduced on the same scale and the final diffraction-angle-dependent intensity,  $I(2\theta)$ , does not require any further absorption correction.

## 1. Introduction

The use of two-dimensional area detectors for powder diffraction has become widespread for various applications with synchrotron radiation (SR), such as high-pressure research (Piltz *et al.*, 1992; Shimomura *et al.*, 1992; Hammersley *et al.*, 1996). Such detectors are used both in transmission and reflection mode with perpendicular and inclined detector geometry at general laboratories (*e.g.* Sulyanov *et al.*, 1994; He, 2003; Rodriguez-Navarro, 2006) and at SR sources with cylindrically curved and flat detectors (*e.g.* Fujiwara *et al.*, 2000; Sulyanov *et al.*, 2011). Details of the geometry refinement are considered by, for example, Hinrichsen *et al.* (2007) and Gommel & Goderis (2010). Specialized software was applied by these authors to perform the transformation from two-dimensional intensities to powder patterns in terms of the diffraction-angle-dependent intensity  $I(2\theta)$ . Averaging over a large solid angle diminishes the coarse-grain and preferred orientation effects and provides high statistical accuracy. The effects of axial divergence, such as line asymmetry and intensity distortions at diffraction angles different from  $90^\circ$ , are removed as each particular pixel is actually a separate detector with a small aperture. Quantitative analysis of diffraction data requires a range of instrumental and geometric corrections for measured intensities, and the absorption correction is one of the most important. A short wavelength is preferable for structure refinement tasks to avoid or facilitate absorption correction problems, but this can be used up to a certain limit only. The absorption correction task requires knowledge of the path length through the specimen and the linear attenuation coef-

ficient at the wavelength used. The intensity is reduced by a factor  $A$  (the transmission factor), given by the formula

$$A = (1/V) \int_V \exp[-\mu(l_1 + l_2)] dV, \quad (1)$$

where  $V$  is the material volume,  $\mu$  the linear attenuation coefficient,  $l_1$  the path length through the absorbing material before the diffraction and  $l_2$  the path length for the diffracted rays. The absorption factor  $A^*$ , the reciprocal of  $A$ , may be found in tabulations such as *International Tables for Crystallography*, Vol. C (Prince, 2004). Specimens with a cylindrical geometry, such as packed capillaries, are common in powder studies, with increased use of capillary stages in laboratory and especially SR diffractometers. Although this is one of the simpler geometries for which to calculate absorption, it does not have a general analytical solution even in the ‘classic’ case when the diffraction is considered only in the plane perpendicular to the cylinder axis. A brief history of the development of this correction is given by Bowden & Ryan (2010). Dwiggins (1972) showed that an analytical solution exists only for two diffraction angles, *i.e.*  $2\theta = 0^\circ$  and  $2\theta = 180^\circ$ . Modern absorption correction tables for the whole  $2\theta$  range are based mainly on work by Dwiggins (1975). These  $A^*$  values were used to verify the quality of the new data obtained by Bowden & Ryan (2010), who applied the numerical integration in the Cartesian coordinate system, and by Ida (2010), who used polar coordinates. The quality of the powder patterns obtained with up-to-date two-dimensional area detectors and SR enable one to achieve good Bragg  $R$  factors, comparable to those obtained by the single-crystal method. However, the absorption factor for two-dimensional area experiments must

be calculated for each particular pixel and not only for the equatorial section using known approaches and tabulations. Clearly inclined rays travel a longer distance through the cylinder (the component along the cylinder axis), *i.e.* absorption varies in the perpendicular direction. To our knowledge this effect has not been respected in the available literature when integrating reflection intensities along the Debye–Scherrer lines over a large solid angle.

Here we use the Cartesian coordinate system to calculate the absorption factor at each pixel by direct computer summation of equation (1). Any diffracted beam coming out of the cylindrical sample in the transmission geometry is defined by the direction cosines in the coordinate system connected with the sample. Such an approach makes our software usable for any type of two-dimensional area detector, including flat, spherical or cylindrical. As modern two-dimensional area detectors have a large number of pixels, interpolation by the triangulation method with a 10–100 pixel grid step size along the coordinate axes in the detector plane

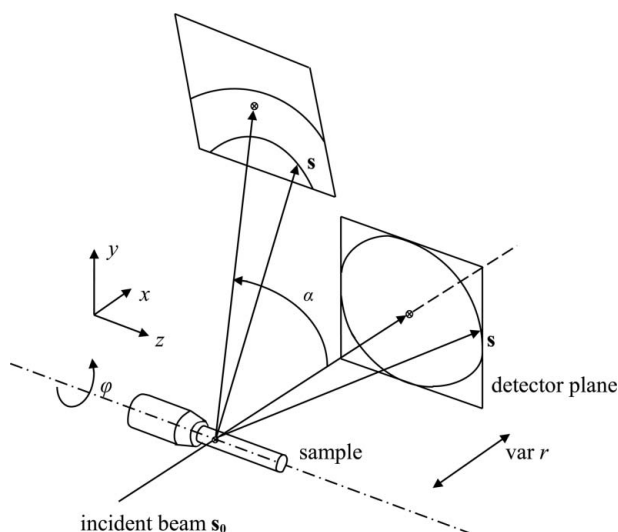


**Figure 1**  
The transmission geometry with a flat two-dimensional area detector.

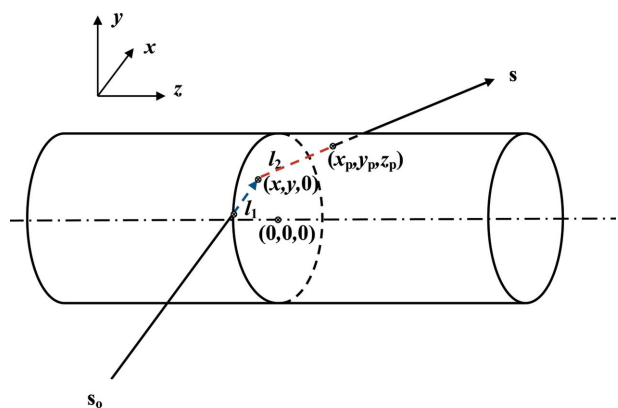


**Figure 2**  
General diffraction scheme for a cylindrical sample.  $s_0$  and  $s$  are the incident and diffracted beam directions, and  $l_1$  and  $l_2$  the corresponding path lengths through the sample before and after the diffraction at the point  $(x, y, 0)$ . The exit point is at  $(x_p, y_p, z_p)$ .

was used to save computer time. Then the diffraction-angle-dependent intensity  $I(2\theta)$  calculated over the whole detector plane enables one to use the Rietveld structure refinement programs without any further absorption correction.

## 2. Calculation procedure

When using two-dimensional area detectors for powder diffraction, one must calculate the absorption factor correction for each particular pixel. The scheme with a scanning two-dimensional area detector for the transmission geometry is shown in Fig. 1. As an example we chose a flat detector, but the procedure is in principle applicable to other types as well. Note that the coordinate system to describe the angular coordinates of each particular pixel may be chosen in different ways, and five parameters are generally required (see *e.g.* Gommel & Goderis, 2010; Sulyanov *et al.*, 2011). To cover larger diffraction angles, the detector is rotated in the vertical plane by the angle  $\alpha$ , which is zero when the detector is set perpendicular to the incident beam. For the absorption factor calculation we chose the system connected with the sample. The incident beam  $s_0$  (Figs. 1 and 2) is directed along the  $x$  axis perpendicular to the cylinder axis (coinciding with the  $z$  axis), and the  $y$  axis is set vertical. The spatial coordinates of a pixel lying on the diffracted beam  $s$  may be represented by the direction cosines  $C_x, C_y, C_z$ . Let the point where the diffraction takes place have the coordinates  $(x, y, z = 0)$  and let  $(x_p, y_p, z_p)$  be the coordinates of the point where the diffracted ray leaves the cylindrical sample having radius  $R$ . Here and in the following derivations we assume the sample-to-detector distance  $r$  to be much larger than the sample diameter, such that deviations of the exact  $2\theta$  angle can be neglected. The distance  $l_1$  passed by the ray within the sample before diffraction is

$$l_1 = (R^2 - y^2)^{1/2} + x. \tag{2}$$

The equation describing points on the cylinder surface is

$$x_p^2 + y_p^2 = R^2. \tag{3}$$

The line of a diffracted ray can be expressed by its parametric equation as

$$\frac{x - x_p}{C_x} = \frac{y - y_p}{C_y} = \frac{z - z_p}{C_z}. \tag{4}$$

It follows that

$$[x - (y - y_p)C_x C_y^{-1}]^2 + y_p^2 = R^2 \tag{5}$$

and  $y_p$  is a variable in the quadratic equation

$$[(C_x C_y^{-1})^2 + 1]y_p^2 + 2C_x C_y^{-1}[x - y C_x C_y^{-1}]y_p + x^2 + y^2(C_x C_y^{-1})^2 - 2xy C_x C_y^{-1} - R^2 = 0. \tag{6}$$

The output point coordinates on the sample surface are

$$y_p = \left( y(C_x C_y^{-1})^2 - x C_x C_y^{-1} \pm \left\{ R^2 [(C_x C_y^{-1})^2 + 1] - [x - y(C_x C_y^{-1})]^2 \right\}^{1/2} \right) / [(C_x C_y^{-1})^2 + 1], \quad (7)$$

$$x_p = x + (y_p - y) C_x C_y^{-1},$$

$$z_p = (y_p - y) C_z C_y^{-1}.$$

Obviously we consider only the solution for  $y_p$  along the direction of the diffracted beam  $\mathbf{s}$  and not the opposite direction, so only the solution with the ‘+’ sign instead of ‘±’ should be taken. The distance  $l_2$  is calculated by the formula

$$l_2 = [(x - x_p)^2 + (y - y_p)^2 + z_p^2]^{1/2}. \quad (8)$$

Using these formulae to calculate the absorption factor by the computer summation method we must, of course, impose the condition that all the points chosen be located within the circular cylinder section. The summation is performed with steps  $\Delta x, y = R/N$ , where  $N$ , the number of divisions along the  $x$  and  $y$  axes, determines the accuracy of the integration.

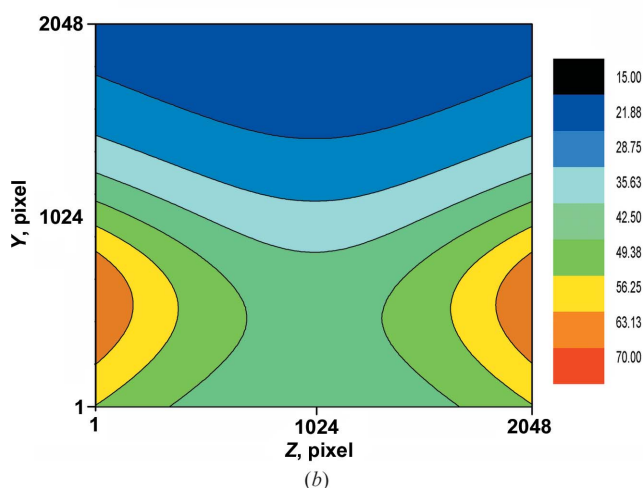
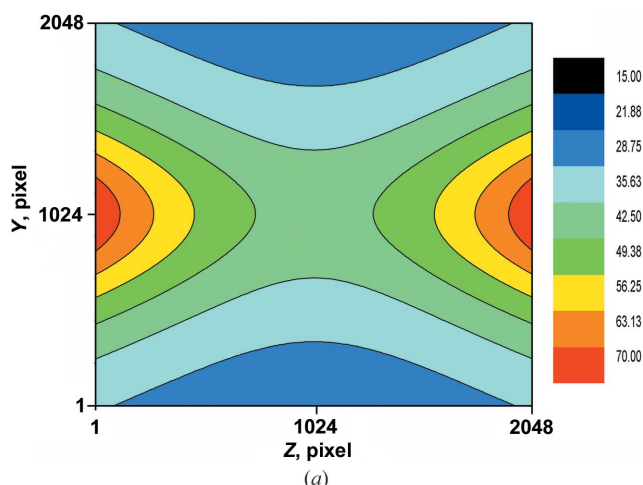


**Figure 3** Contour map of the absorption factor distribution over a two-dimensional area-detector plane for  $\mu R = 2.5$ . (a) Perpendicular geometry ( $\alpha = 0^\circ$ ), (b) inclined geometry ( $\alpha = 30^\circ$ ).

Modern two-dimensional area detectors have a large number of pixels, for example  $2048 \times 2048$ . As an example we calculated the absorption factor for  $\mu R = 2.5$  with the detector set at a distance from the cylindrical sample equivalent to 1000 pixels, the sample projection onto the detector plane being at pixel (1024, 1024). The result of such a calculation is presented in Fig. 3 for the perpendicular and inclined geometry. To estimate the quality of these calculations we used different division numbers  $N$  for the pixel at  $2\theta = 0^\circ$  and compared the results with the analytical solution ( $A^* = 40.09687$ ) obtained by Dwiggin (1972). Fig. 4 demonstrates the relative difference between calculated and analytical  $A^*$  values. It is seen that it is quite sufficient to take moderate  $N$  values of about 1000 points. In this case the relative error is  $\Delta A^*/A^* = 0.04\%$  (0.005% for  $N = 8000$ ). Fig. 5(a) shows several sections, one pixel wide, of the  $A^*$  surface calculated for inclined ( $\alpha = 45^\circ$ ) geometry at detector coordinates  $z = 1024, 1224, 1424, 1624$  and 1824 pixels, corresponding to rotation angles 0, 11.3, 21.8, 31.0 and  $38.7^\circ$ , respectively. The line at  $z = 1024$  pixels (rotation angle zero) fits perfectly with the data points (squares) taken from Dwiggin (1975), *i.e.* the ‘in-plane’ distribution, which depends on the diffraction angle only, thereby validating our approach. However, it is seen that the absorption factor distribution in the lateral directions can substantially differ from the values along the central line of the detector. Fig. 5(b) demonstrates the appreciable variation along the Debye–Scherrer rings for a flat detector at  $\alpha = 0$ . Note that this becomes more serious for larger  $2\theta$  angles. So, at least for not very small values of  $\mu R$ , one must take into account this more complicated calculation of the absorption factor over the whole detector surface to obtain accurate results.

### 3. Triangulation method to reduce the calculation time

The calculation time can be large even for the ‘in-plane’ case (Bowden & Ryan, 2010), if quite small division steps are used, such as  $N = 1000$  and larger. In the two-dimensional area

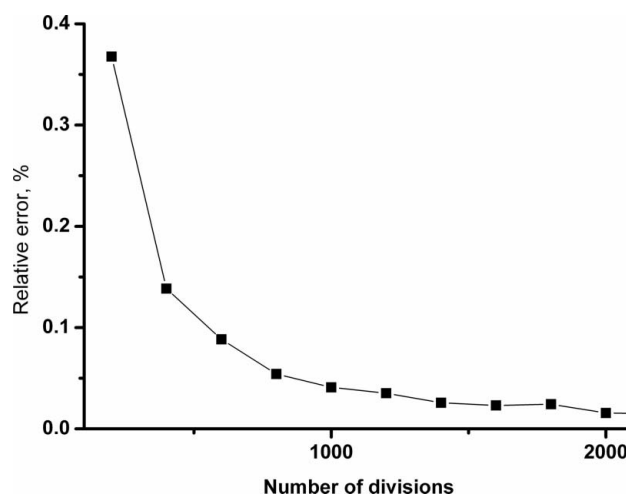


**Figure 4** The relative difference between calculated and analytical values of the absorption factor for  $\mu R = 2.5$  at  $2\theta = 0^\circ$  as a function of the number of summation steps.

registration case the number of pixels can be more than  $10^7$ , which would require unacceptably long computer times. Therefore, an interpolation procedure should be applied to reduce the number of points where the absorption factor is calculated explicitly. One of the simplest ways is to apply a triangulation procedure, *i.e.* to calculate the absorption factor only at the points of a square grid chosen on the two-dimensional area-detector plane and then to apply an interpolation procedure, for example, for upper-left triangle and lower-right triangle (note that the triangles have a conjoint hypotenuse), to describe the absorption factor in the inner part between the four vertices. We used the equation for an interpolation plane passing through three vertex points of such triangles to calculate the absorption factor for the inner points. We chose a  $10 \times 10$  square grid, thus actually reducing the number of points for calculation by a factor of 100. The two-dimensional area map of the relative difference between two calculations, *i.e.* full pixel-by-pixel and with interpolation, for the perpen-

dicular geometry of Fig. 3(a) is shown in Fig. 6. The mean relative deviation over the whole detector plane is 0.046% and the maximum deviation is 0.31%. Additionally, for section 1 of Fig. 5(a) we calculated the difference for  $A^*$  obtained directly for each point and with the use of the triangulation procedure. This typical oscillatory behaviour (for a piece of the section) is shown in Fig. 7.

#### 4. Experimental validation

In order to test our software a NIST N660a standard  $\text{LaB}_6$  sample packed in a 0.2 mm glass capillary was measured at the ‘Belok’ station on the source from a bending magnet (Kurchatov Centre, Moscow) which is designed for protein crystals and equipped with a Marresearch CCD Rayonix SX165 detector ( $2048 \times 2048$ ). The wavelength was  $\lambda = 0.9835 \text{ \AA}$ , so the theoretical  $\mu R = 2.05$  assuming 60%  $\text{LaB}_6$

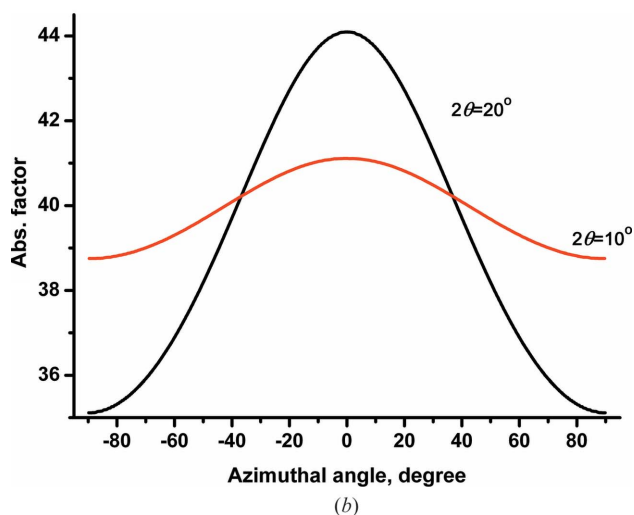
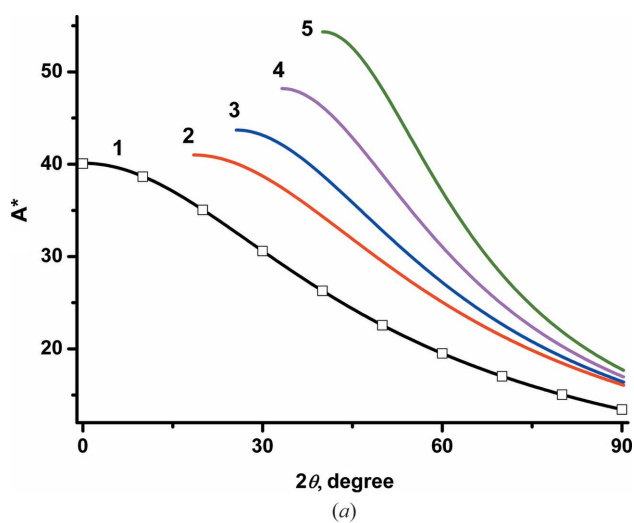


**Figure 5** Sections of the  $A^*$  surface with  $\mu R = 2.5$ . (a) Linear sections by planes parallel to the  $y$  axis ( $\alpha = 45^\circ$ ) at (1)  $z = 1024$ , (2) 1224, (3) 1424, (4) 1624 and (5) 1824 pixels. The squares correspond to the values obtained by Dwiggins (1975) for the common ‘in-plane’ case. (b) Circular sections at  $2\theta = 10^\circ$  and  $20^\circ$  ( $\alpha = 0^\circ$ ).

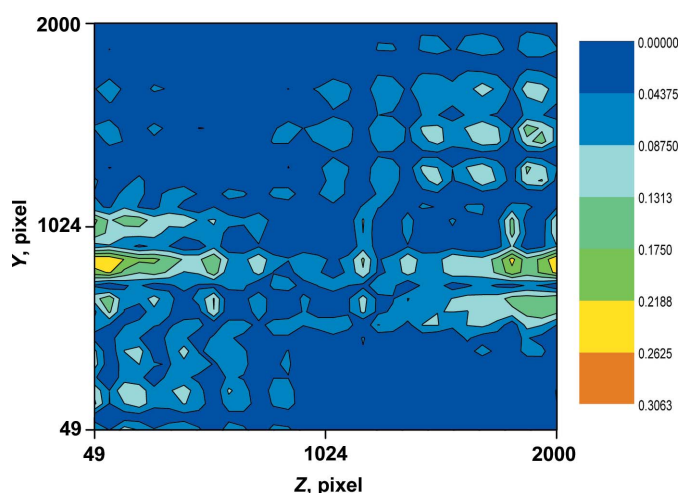


**Figure 6** Contour map of the relative difference (in %) between the absorption factors calculated for each particular pixel and obtained by the triangulation method with a  $10 \times 10$  grid.

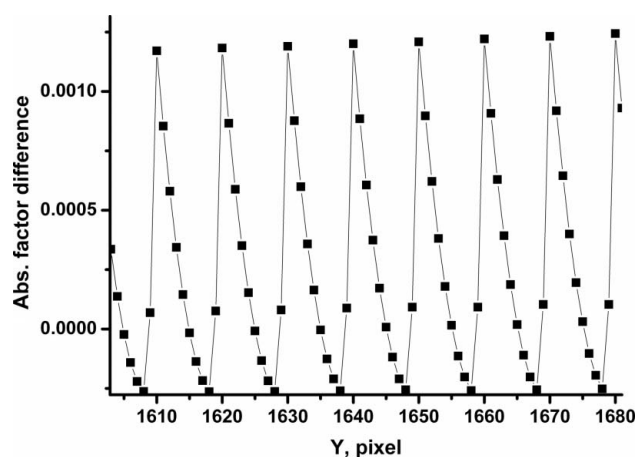


**Figure 7** Absolute difference of the absorption factor as calculated for each particular pixel and obtained by triangulation with  $10 \times 10$  grid points along the strip with  $z = 1024$ .

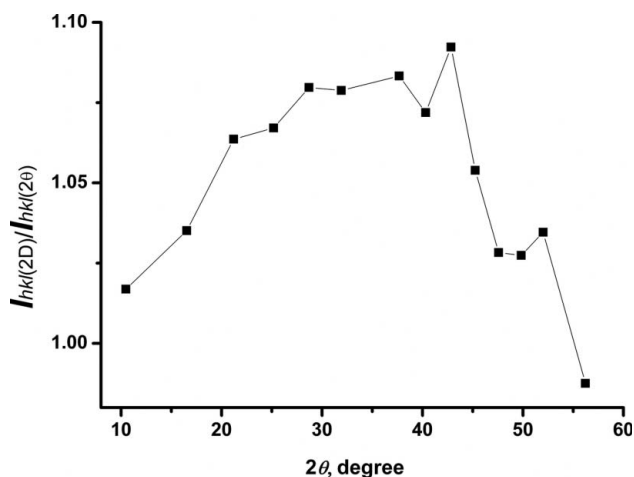


**Figure 8**  
The ratios of the Bragg peak intensities of  $\text{LaB}_6$  obtained with the 'standard' and 'new' absorption correction procedures.

single-crystal density. The detector was set at  $r = 150$  mm and the maximum rotation angle  $\alpha = 29^\circ$ . Powder patterns were calculated over the whole detector plane with a round entrance window. The polarization factor was taken as  $P = 0.95$ . The diffraction-angle range was  $5\text{--}58^\circ$ , so only the first 14 Bragg peaks were registered. Two different  $I(2\theta)$  patterns were calculated: (1) with the absorption correction for each particular pixel depending only on the  $2\theta$  angle by simple linear interpolation using the 'in-plane' dependence with step  $\Delta 2\theta = 1^\circ$ ; (2) with the correction as described above (denoted 2D). Then the integrated Bragg peak intensities were obtained by pseudo-Voigt function fitting for both approaches. The resulting ratio  $I_{hk(2D)}/I_{hk(2\theta)}$  is presented in Fig. 8. It is seen that the difference is largest (amounting to about 8%) closer to the middle of the range and it is almost zero near the ends. This is explained by the fact that there is less lateral angular spread of the Bragg curves in the upper and lower (from the central horizontal line) detector parts. It may be worth mentioning that, by varying the  $\mu R$  coefficient in these calculations, one can determine its value as that at which the intensity variance along the Bragg curves is minimum.

## 5. Concluding remarks

In this work it is shown that, if a two-dimensional area detector is applied for powder diffraction, standard absorption factor tabulations become unusable for larger values of  $\mu R$ . A computer program was written to calculate the absorption factor at each detector pixel before the transformation from two-dimensional area histogram to the  $I(2\theta)$  patterns. In this case no further absorption correction is required. The Fortran code is available from the authors. It consists of three parts. The first part calculates the direction cosines  $C_x$ ,  $C_y$ ,  $C_z$  for each pixel (three  $2048 \times 2048$  matrices) for a particular geometry defined in the preliminary prepared data file. The second part calculates the  $A^*$  values for  $205 \times 205$  grid points. This procedure takes about 2 h on a typical modern PC for  $N = 1000$  (about 0.2 s for one pixel). The third part performs the triangulation interpolation and saves the whole correction matrix for further use.

## References

- Bowden, M. & Ryan, M. (2010). *J. Appl. Cryst.* **43**, 693–698.  
 Dwiggin, C. W. (1972). *Acta Cryst.* **A28**, 219–220.  
 Dwiggin, C. W. (1975). *Acta Cryst.* **A31**, 146–148.  
 Fujiwara, A. *et al.* (2000). *J. Appl. Cryst.* **33**, 1241–1245.  
 Gommès, C. J. & Goderis, B. (2010). *J. Appl. Cryst.* **43**, 352–355.  
 Hammersley, A. P., Svensson, S. O., Hanfland, M., Fitch, A. N. & Häusermann, D. (1996). *High Pres. Res.* **14**, 235–248.  
 He, B. B. P. (2003). *Powder Diffr.* **18**, 71–85.  
 Hinrichsen, B., Dinnebier, R. E. & Jansen, M. (2007). *Z. Kristallogr. Suppl.* **26**, 215–220.  
 Ida, T. (2010). *J. Appl. Cryst.* **43**, 1124–1125.  
 Prince, E. (2004). Editor. *International Tables for Crystallography*, Vol. C, *Mathematical, Physical and Chemical Tables*. Dordrecht: Kluwer Academic Publishers.  
 Piltz, R. O., McMahon, M. I., Crain, J., Hatton, P. D., Nelmes, R. J., Cernik, R. J. & Bushnell-Wye, G. (1992). *Rev. Sci. Instrum.* **63**, 700–703.  
 Rodríguez-Navarro, A. B. (2006). *J. Appl. Cryst.* **39**, 905–909.  
 Shimomura, O., Takemura, K., Fujihisa, H., Fujii, Y., Ohishi, Y., Kikegawa, T., Amemiya, Y. & Matsushita, T. (1992). *Rev. Sci. Instrum.* **63**, 967–973.  
 Sulyanov, S., Boysen, H., Paulmann, C., Sulyanova, E. & Rusakov, A. (2011). *Z. Kristallogr. Proc.* **1**, 175–180.  
 Sulyanov, S. N., Popov, A. N. & Kheiker, D. M. (1994). *J. Appl. Cryst.* **27**, 934–942.